

N -continuous Aided GFDM Signaling

Peng Wei, Yue Xiao, Lilin Dan

Abstract

An N -continuous-based generalized frequency division multiplexing (GFDM) transceiver architecture is investigated, which operates with the aid of time-domain N -continuous orthogonal frequency division multiplexing (TD-NC-OFDM), hence called time-domain N -continuous GFDM (TD-NC-GFDM). More specifically, the basis signals conceived allow us to attain compact spectrum as an explicit benefit of sidelobe suppression, which constitute the smooth signal capable of eliminating the discontinuities imposed by the cyclic shift GFDM filters and their high-order derivatives. The proposed N -continuous GFDM signaling has relatively low interference through evaluating the signal-to-interference ratio (SIR) that significantly decreases upon increasing the number of GFDM subsymbols. Furthermore, a signal recovery algorithm for reception is adopted by constructing a decoding matrix for eliminating the interference caused by the smooth signal, which exhibits an explicit error performance improvement compared to TD-NC-OFDM. It is demonstrated that N -continuous GFDM outperforms TD-NC-OFDM in terms of sidelobe suppression, while achieving small BER performance degradation with a small roll-off filter compared to original OFDM.

Index Terms

Generalized frequency division multiplexing (GFDM), N -continuous, sidelobe suppression, spectral leakage, time-domain N -continuous orthogonal frequency division multiplexing (TD-NC-OFDM).

I. INTRODUCTION

Generalized frequency division multiplexing (GFDM) relying on flexible waveforms in time and frequency has been paid more attention in the 5th generation cellular networks [1]–[19], particularly in scenarios such as high data rate communications [17], [19] and low latency communications [4], [13], [17], since it has a promising spectral efficiency thanks to the reduced burden on guard interval and the low spectral leakage, which is also called out-of-band power radiation, generated from the superposition of the power of sidelobes in frequency domain. GFDM exhibits a strong frequency localization on the individual subcarrier [15], however, for a block of continuous subcarriers, its sidelobe suppression performance is limited due to the discontinuities caused by the circularly shaped waveforms of the transmitter filter [13], [16]–[18]. Hence, the data transmission over the adjacent channels is interfered.

P. Wei is with the School of Electronics and Information Engineering, Tianjin Polytechnic University, Tianjin, China (e-mail: wpwwwhttp@163.com).

Y. Xiao and L. Dan are with the National Key Laboratory of Science and Technology on Communications, University of Electronic Science and Technology of China, Chengdu, China (e-mail: {xiaoyue, lilindan}@uestc.edu.cn).

To mitigate this limitation, it is beneficial to employ powerful schemes for the smoothness enhancement of the GFDM signal. A classic solution conceived for generating the smooth edges is to employ windowing technique [17], [18], that of multiplying a window on each guard-interval-assisted GFDM symbol. However, for the robust against multipath channel effect, the extended guard interval results in a reduction in spectral efficiency. Furthermore, the inherent non-orthogonality of the window may impose a bit error ratio (BER) performance degradation. In [19], one or more zero-valued guard symbols are inserted into boundaries of each GFDM symbol to eliminate the abrupt change between two consecutive GFDM symbols and achieve more smooth transitions. Unfortunately, a significant reduction of spectral efficiency is caused when the number of the GFDM sub-symbols per GFDM symbol is small, where a small error performance degradation will be guaranteed as proved in [5]. Generally, the aforementioned sidelobe suppression techniques were developed in terms of the time-domain continuity. However, when considering the GFDM signal with a block of subcarriers, having many circularly shifted versions of the prototype filter [17], the non-smoothness of the GFDM signal may not be directly cancelled, where the non-smoothness is described as the discontinuities of a signal and its high-order derivatives.

To provide further insights, by improving continuities of the OFDM signal and its first N derivatives, termed as N -continuous, Ref. [20] proposes the N -continuous OFDM (NC-OFDM) technique for a considerable suppression of out-of-band power radiation over a block of subcarriers, while having the same spectral efficiency as conventional OFDM [13]. Since the main challenges of the NC-OFDM technique are high complexity and severe interference, it is of paramount importance to develop a reduced-complexity and low-interference scheme. In [21], the improved technique nulls the spectrum at several chosen frequencies and exhibits complexity reduction, but causing BER performance degradation. Ref. [22] gives a precoder to enhance the BER performance compared to [21], but results in data rate loss.

Most recently, the time-domain N -continuous OFDM (TD-NC-OFDM) techniques were invoked by conventional NC-OFDM [20] for the N -continuous implementation in the time domain for the first time [23], [24]. Owing to the explicit benefits of utilization of time-domain OFDM waveforms, this technique allows us to effectively eliminate the discontinuities in the time domain, while maintaining a low complexity. Unfortunately, the TD-NC-OFDM technique may fail to mitigate the severe interference imposed by a smooth signal for suppressing the spectral leakage as good as the conventional NC-OFDM.

Against this background, our novel contributions are that we further expand the N -continuous concept and propose an N -continuous GFDM signal architecture, in order to effectively eliminate the discontinuities of the GFDM signal and its high-order derivatives, and hence significantly reduce the spectral leakage, while N -continuous GFDM maintains the same spectral efficiency as conventional GFDM. Three aspects highlight the novel properties of the proposed N -continuous GFDM.

- 1) Motivated by both the benefits and limitations of the TD-NC-OFDM technique [24], using the time and frequency properties of the GFDM waveforms, we design a time-domain N -continuous-aided GFDM signaling, which allows us to give the generalized basis signals in a new basis set and reduce the non-smoothness imposed by the original GFDM transmit filters.
- 2) Furthermore, we analyze the interference of the time-domain N -continuous GFDM (TD-NC-GFDM) signal,

which is proved to attain a considerable signal-to-interference ratio (SIR) outperforming TD-NC-OFDM when the number of GFDM subsymbols per GFDM symbol is bigger than 1 and the GFDM signal has the same number of subcarriers as the OFDM counterpart.

- 3) Finally, an iterative signal recovery algorithm for the received N -continuous GFDM signal is investigated based on constructing a decoding matrix.

The remainder of the paper is organized as follows. In Section II, conventional GFDM transmitter and receiver are introduced, and the spectral limitation of the GFDM signal is analyzed. In Section III, we detail our N -continuous GFDM model at the transmitter, followed by the signal recovery algorithm at the receiver and the SIR analysis. Simulation results are investigated in Section IV. Finally, in Section V, this paper is concluded.

II. GFDM SYSTEM

Here, we first detail the GFDM transmitter, and then, introduce three common GFDM demodulators at the receiver. Finally, the problem caused by the conventional GFDM transmit filters is investigated.

A. GFDM Transmitter

In GFDM transmitter, bit streams are first modulated to complex symbols $d_{i,k,m}$ that are divided into sequences of KM symbols long in the i th GFDM symbol. Each sequence (as a vector) $\mathbf{d}_i = [\mathbf{d}_{i,0}^T, \mathbf{d}_{i,1}^T, \dots, \mathbf{d}_{i,M-1}^T]^T$ with $\mathbf{d}_{i,m} = [d_{i,0,m}, d_{i,1,m}, \dots, d_{i,K-1,m}]^T$, $m = 0, 1, \dots, M-1$, is spread on K subcarriers in M time slots. Therein, $d_{i,k,m}$ is the transmitted data on the k th subcarrier in the m th subsymbol of the i th GFDM symbol block. Consider that the data symbols $d_{i,k,m}$ are taken from an independent and identically distributed (i.i.d.) process with the zero mean and the unit variance. Each $d_{i,k,m}$ is transmitted through a pulse shaping filter [17]

$$g_{k,m}(n) = g((n - mK)_N) e^{-j2\pi \frac{k}{K}n}, \quad (1)$$

where the signal sample index is $n = 0, 1, \dots, N-1$ with $N = KM$, $(\cdot)_N$ denotes the modulo of N , and $g(n)$ is a prototype filter whose time and frequency shifts by k and m are $g_{k,m}(n)$. By the superposition of all the filtered $d_{i,k,m}$, the GFDM signal is represented by

$$x_i(n) = \sum_{k=0}^{K-1} \sum_{m=0}^{M-1} d_{i,k,m} g_{k,m}(n), \quad (2)$$

and its implementation is shown in Fig. 1 that is the same as the transmitter shown in [17]. Eq. (2) can be rewritten in the matrix form as

$$\mathbf{x}_i = \mathbf{A} \mathbf{d}_i, \quad (3)$$

where \mathbf{A} is an $N \times N$ transmitter matrix [17], given by

$$\mathbf{A} = [\mathbf{g}_{0,0} \ \cdots \ \mathbf{g}_{K-1,0} \ \mathbf{g}_{0,1} \ \cdots \ \mathbf{g}_{K-1,M-1}] \quad (4)$$

with $\mathbf{g}_{k,m} = [g_{k,m}(0), g_{k,m}(1), \dots, g_{k,m}(N-1)]^T$.

Lastly, after a cyclic prefix (CP) of N_{cp} samples is appended to \mathbf{x}_i , the transmitted GFDM signal in the time range $(-\infty, +\infty)$ is expressed as

$$x(n) = \sum_{i=-\infty}^{+\infty} \sum_{k=0}^{K-1} \sum_{m=0}^{M-1} d_{i,k,m} g_{k,m}(n - i(N + N_{cp})). \quad (5)$$

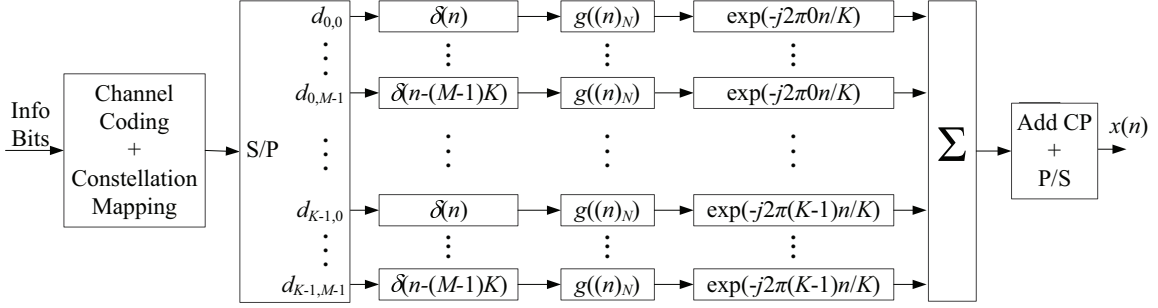


Fig. 1. Block diagram of GFDM transmitter.

B. GFDM Receiver

At the receiver, the i th corresponding received GFDM signal is

$$y_i(n) = h_i(n) * x_i(n) + n_i(n), \quad (6)$$

where $*$ denotes the linear convolution operation, $h_i(n)$ is the channel response in the time domain, and $n_i(n)$ denotes the complex-valued additive white Gaussian noise (AWGN) with zero mean and variance σ^2 .

Under the assumption of perfect synchronization between the transmitter and the receiver, after the CP is removed, Eq. (6) can be expressed in the matrix form as

$$\mathbf{y}_i = \mathbf{H}_i \mathbf{x}_i + \mathbf{n}_i, \quad (7)$$

where $\mathbf{y}_i = [y_i(0), y_i(1), \dots, y_i(N-1)]^T$, $\mathbf{n}_i = [n_i(0), n_i(1), \dots, n_i(N-1)]^T$, and \mathbf{H}_i denotes the $N \times N$ channel matrix which is a circular convolution matrix.

According to [17], three linear GFDM demodulators have been considered, which are matched filter (MF), zero-forcing (ZF), and minimum mean square error (MMSE) receivers. Suppose that zero-forcing channel equalization is adopted. The estimated data $\hat{\mathbf{d}}_i$ by the three receivers can be, respectively, expressed by

$$\hat{\mathbf{d}}_{i,\text{MF}} = \mathbf{A}^H \mathbf{H}_i^{-1} \mathbf{y}_i, \quad (8a)$$

$$\hat{\mathbf{d}}_{i,\text{ZF}} = \mathbf{A}^{-1} \mathbf{H}_i^{-1} \mathbf{y}_i, \quad (8b)$$

$$\hat{\mathbf{d}}_{i,\text{MMSE}} = (\mathbf{R}_{i,n} + \mathbf{A}^H \mathbf{H}_i^H \mathbf{H}_i \mathbf{A})^{-1} \mathbf{A}^H \mathbf{H}_i^H \mathbf{y}_i, \quad (8c)$$

where $\mathbf{R}_{i,n}$ is the covariance matrix of the channel noise.

Finally, the data $\hat{\mathbf{d}}_i$ are demapped to a sequence of bits by a decoder.

C. Problem of Spectral Leakage

For the discontinuities between two consecutive GFDM symbols caused by the circularly shaped transmitter filters $g_{k,m}(n)$ in (1), the GFDM signal has a limited sidelobe suppression performance, where the discontinuity is described by the abrupt changes of amplitude and phase. In this case, corresponding to (2), each continuous-time GFDM symbol can be considered to be windowed by a rectangular window $R(t)$, expressed as

$$x_i(t) = \sum_{k=0}^{K-1} \sum_{m=0}^{M-1} d_{i,k,m} g(t - mT_s) e^{-j2\pi \frac{k}{T_s} t} R(t), \quad (9)$$

where T_s is the time duration of a GFDM subsymbol, T_{cp} is the CP duration, and when $-T_{cp} \leq t \leq MT_s$, $R(t) = 1$ and else $R(t) = 0$. We assume that $E\{|d_{i,k,m}|^2\} = 1$, similar to [17], the power spectral density (PSD) of the baseband GFDM signal can be calculated by

$$P(f) = \lim_{i \rightarrow \infty} \left(\frac{E\{|\mathcal{F}\{x_i(t)\}|^2\}}{MT_s + T_{cp}} \right) = \frac{1}{MT_s + T_{cp}} \sum_{k,m} \left| \text{sinc}(f(MT_s + T_{cp})) * G_{k,m} \left(f - \frac{k}{T_s} \right) \right|^2, \quad (10)$$

where $\mathcal{F}\{\cdot\}$ is the Fourier transform operation, $G_{k,m}(f)$ is the Fourier transform of $g_{k,m}(t)$, and $\text{sinc}(x) \triangleq \sin(\pi x)/(\pi x)$.

It is denoted in (58) that the sidelobe of the baseband GFDM signal is affected by both the transmit filter $G_{k,m}(f)$ and the sinc waveform. Due to the slow sidelobe decaying of the sinc waveform, the spectral leakage of the baseband GFDM signal cannot be significantly reduced, but since the transmit filter $G_{k,m}(f)$ has the steep sidelobe decaying, it is much lower than that of the rectangularly pulsed OFDM decaying as the sinc waveform. Additionally, when the number of subcarriers is increased, the increase in the number of circularly shifted transmitter filters will increase the discontinuities between two consecutive GFDM symbols, which may degrade the performance of sidelobe suppression. Thus, to solve the problems above, an N -continuous scheme for the GFDM signals will be proposed below for achieving a notably compact spectrum.

III. N -CONTINUOUS GFDM

In this section, invoked by TD-NC-OFDM, we first formulate N -continuous GFDM to how to improve the smoothness of the GFDM signal. Then, a signal recovery algorithm is investigated via a designed decoding matrix for the interference cancellation. Lastly, the effect of the smooth signal on the GFDM system is evaluated in terms of SIR.

A. Transmitter

To enhance the smoothness of the GFDM signal, based on [20], [23], [24], the continuities of the high-order derivatives of the GFDM signal are required. According to [23], [24], by adding a smooth signal $w_i(n)$ in each GFDM symbol, that is

$$\bar{x}_i(n) = x_i(n) + w_i(n), \quad (11)$$

the transmit GFDM signal $x(n)$ in (5) becomes N -continuous. The smooth signal $w_i(n)$ should satisfy

$$w_i^{(v)}(n) \Big|_{n=-N_{cp}} = \bar{x}_{i-1}^{(v)}(n) \Big|_{n=N} - x_i^{(v)}(n) \Big|_{n=-N_{cp}} \quad (12)$$

for $n \in \mathcal{N} = \{-N_{\text{cp}}, -N_{\text{cp}} + 1, \dots, N - 1\}$ in the equivalent-baseband GFDM signal with the CP, where $x_i^{(v)}(n)$ is the v th-order derivative of $x_i(n)$ with $v \in \mathcal{U}_V \triangleq \{0, 1, \dots, V\}$ and the highest derivative order (HDO) V .

The smooth signal $w_i(n)$ is designed by a linear combination of basis signals $f_v(n)$ as

$$w_i(n) = \sum_{v=0}^V b_{i,v} f_v(n). \quad (13)$$

To generate $w_i(n)$, how to attain the basis signal $f_v(n)$ and the linear combination coefficients $b_{i,v}$ will be detailed in the following, respectively.

For $f_v(n)$, it belongs to a basis set \mathcal{Q} , which is expressed by

$$\mathcal{Q} = \left\{ \mathbf{q}_{\tilde{v}} \mid \mathbf{q}_{\tilde{v}} = [f_{\tilde{v}}(-N_{\text{cp}}), f_{\tilde{v}}(-N_{\text{cp}} + 1), \dots, f_{\tilde{v}}(N - 1)]^T, \tilde{v} \in \mathcal{U}_{2V} \right\}. \quad (14)$$

For the introduced filters $g_{k,m}(n)$ in the GFDM transmitter, the design of the basis signal is partly different from the counterpart in [24], where there are no the filters $g_{k,m}(n)$. Therein, based on the prototype filter $g(n)$, a generalized design of the basis signal $f_{\tilde{v}}(n)$ is given by

$$f_{\tilde{v}}(n) = \frac{1}{N} \sum_{l=0}^{N-1} \left(j2\pi \frac{l}{N} \right)^{\tilde{v}} F_0(l) e^{j2\pi \frac{n+N_{\text{cp}}}{N} l}, \quad (15)$$

where $F_0(l)$ is the N -point DFT of $f_0(n)$, that is

$$F_0(l) = \sum_{n=0}^{N-1} f_0(n) e^{-j2\pi \frac{n}{N} l},$$

and $f_0(n)$ is a synthesis waveform by summing the K frequency-shifted prototype filter $g(n)$ as

$$f_0(n) = \sum_{k=0}^{K-1} g(n) e^{-j2\pi \frac{k}{K} n}.$$

In this case, $f_{\tilde{v}}(n)$ is the \tilde{v} th-order derivative of $f_0(n)$ in (15).

To calculate $b_{i,v}$, we first rewrite (13) in the matrix form as

$$\mathbf{w}_i = \mathbf{Q} \mathbf{b}_i, \quad (16)$$

where $\mathbf{w}_i = [w_i(0), w_i(1), \dots, w_i(N-1)]^T$, $\mathbf{Q} = [\mathbf{q}_0 \ \mathbf{q}_1 \ \dots \ \mathbf{q}_V]$ and $\mathbf{b}_i = [b_{i,0}, b_{i,1}, \dots, b_{i,V}]^T$. Then, substituting (11) and (13) into (12), we have

$$\mathbf{P}_f \mathbf{b}_i = \Delta \mathbf{x}_i, \quad (17)$$

where \mathbf{P}_f is a $(V+1) \times (V+1)$ symmetric matrix given as

$$\mathbf{P}_f = \begin{bmatrix} f(-N_{\text{cp}}) & f_1(-N_{\text{cp}}) & \dots & f_V(-N_{\text{cp}}) \\ f_1(-N_{\text{cp}}) & f_2(-N_{\text{cp}}) & \dots & f_{V+1}(-N_{\text{cp}}) \\ \vdots & \vdots & & \vdots \\ f_V(-N_{\text{cp}}) & f_{V+1}(-N_{\text{cp}}) & \dots & f_{2V}(-N_{\text{cp}}) \end{bmatrix}, \quad (18)$$

and since the rows of \mathbf{P}_f are linearly uncorrelated and so are its columns, its inverse \mathbf{P}_f^{-1} exists. On the other hand, the vector

$$\Delta \mathbf{x}_i = \left[\bar{x}_{i-1}(N) - x_i(-N_{\text{cp}}), \bar{x}_{i-1}^{(1)}(N) - x_i^{(1)}(-N_{\text{cp}}), \dots, \bar{x}_{i-1}^{(V)}(N) - x_i^{(V)}(-N_{\text{cp}}) \right]^T,$$

denoting the differences between the GFDM signals and their first V derivatives at the adjacent point between two consecutive GFDM symbols, can be calculated by

$$\Delta \mathbf{x}_i = \mathbf{P}_1 \bar{\mathbf{d}}_{i-1} - \mathbf{P}_2 \mathbf{d}_i, \quad (19)$$

where $\bar{\mathbf{d}}_{i-1} = \mathbf{d}_{i-1} + \mathbf{A}^{-1} \mathbf{w}_{i-1}$. Thus, Eq. (19) can be rewritten as

$$\Delta \mathbf{x}_i = \mathbf{P}_1 \mathbf{d}_{i-1} + \mathbf{P}_1 \mathbf{A}^{-1} \mathbf{w}_{i-1} - \mathbf{P}_2 \mathbf{d}_i \quad (20)$$

with

$$\mathbf{P}_1 = \mathbf{B} \mathbf{G} \quad (21)$$

and

$$\mathbf{P}_2 = \mathbf{B} \Phi \mathbf{G}, \quad (22)$$

where

$$\mathbf{B} = \frac{1}{N} \begin{bmatrix} 1 & 1 & \cdots & 1 \\ j2\pi \frac{0}{N} & j2\pi \frac{1}{N} & \cdots & j2\pi \frac{N-1}{N} \\ \vdots & \vdots & & \vdots \\ (j2\pi \frac{0}{N})^V & (j2\pi \frac{1}{N})^V & \cdots & (j2\pi \frac{N-1}{N})^V \end{bmatrix}, \quad (23)$$

$$\mathbf{G} = [\mathbf{G}_{0,0} \quad \cdots \quad \mathbf{G}_{K-1,0} \quad \cdots \quad \mathbf{G}_{0,M-1} \quad \cdots \quad \mathbf{G}_{K-1,M-1}] = \mathbf{F} \mathbf{A}, \quad (24)$$

\mathbf{F} is an N -point DFT matrix with its $(l+1)$ th row and $(n+1)$ th column element $e^{-j2\pi \frac{l}{N} n}$ for $l, n = 0, 1, \dots, N-1$, $\mathbf{G}_{k,m} = [G_{k,m}(0), G_{k,m}(1), \dots, G_{k,m}(N-1)]^T$, $G_{k,m}(l)$ is the N -point DFT of $g_{k,m}(n)$,

$$\Phi = \text{diag} \left(e^{j\varphi^0} \ e^{j\varphi^1} \ \dots \ e^{j\varphi^{(N-1)}} \right), \quad (25)$$

and $\varphi = -2\pi N_{\text{cp}}/N$.

Thus, from (17), (18), and (20), \mathbf{b}_i can be calculated by

$$\mathbf{b}_i = \mathbf{P}_f^{-1} (\mathbf{P}_1 \mathbf{d}_{i-1} + \mathbf{P}_1 \mathbf{A}^{-1} \mathbf{w}_{i-1} - \mathbf{P}_2 \mathbf{d}_i). \quad (26)$$

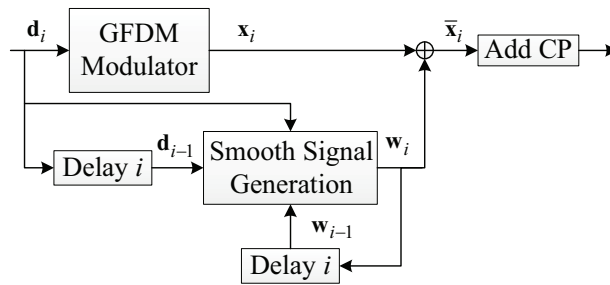


Fig. 2. Block diagram of the N -continuous GFDM transmitter.

Finally, according to (11), (16), and (26), as shown in Fig. 2, the N -continuous GFDM signal is expressed by

$$\bar{\mathbf{x}}_i = \mathbf{x}_i + \mathbf{Q} \mathbf{P}_f^{-1} (\mathbf{P}_1 \mathbf{d}_{i-1} + \mathbf{P}_1 \mathbf{A}^{-1} \mathbf{w}_{i-1} - \mathbf{P}_2 \mathbf{d}_i), \quad (27)$$

where when $i = 0$, \mathbf{w}_i is initialized as an $N \times 1$ all-zero vector $\mathbf{0}_{N \times 1}$, that is $\bar{\mathbf{d}}_0 = \mathbf{d}_0$.

B. Signal Recovery Algorithm

At the receiver side, to cancel the interference of the smooth signal, an iterative signal recovery algorithm is proposed with the aid of the decoding matrix used for the reconstruction of the smooth signal.

With the same synchronization assumption as (7), after removing CP and equalizing the channel effect by ZF, the received N -continuous GFDM signal is expressed by

$$\tilde{\mathbf{y}}_i = \bar{\mathbf{x}}_i + \mathbf{H}_i^{-1} \mathbf{n}_i. \quad (28)$$

Then, our goal is to cancel the estimated smooth signal from the received N -continuous GFDM signal $\tilde{\mathbf{y}}_i$. Without the loss of generality, the ZF demodulator in (8) is employed at the receiver. The estimated signal $\hat{\mathbf{y}}_{i,(r)}$ in the r th iteration of the signal recovery algorithm can be formulated as

$$\hat{\mathbf{y}}_{i,(r)} = \mathbf{A}^{-1} (\tilde{\mathbf{y}}_i - \mathbf{w}_{i,(r)}), \quad (29)$$

where the r th estimated smooth signal $\mathbf{w}_{i,(r)}$ is

$$\mathbf{w}_{i,(r)} = \mathbf{P}_w (\mathbf{A}^{-1} \tilde{\mathbf{y}}_i) - \mathbf{Q} \mathbf{P}_f^{-1} \mathbf{P}_2 \hat{\mathbf{d}}_{i,(r-1)} \quad (30)$$

with the decoding matrix \mathbf{P}_w constructed as

$$\mathbf{P}_w = \mathbf{Q} \mathbf{P}_f^{-1} \mathbf{P}_2, \quad (31)$$

which is proved as follows.

Proof: Our proof is based on necessary condition and sufficient condition.

1) Necessary Proof

We first give the initialization of $\hat{\mathbf{d}}_{i,(r)} = \mathbf{0}_{N \times 1}$ for $r = 0$. According to the design of the smooth signal in (26) (or (19)), the i th smooth signal is related to the $(i-1)$ th and i th GFDM symbols. Thus, for the reconstruction of the smooth signal, the key is how to extract the $(i-1)$ th GFDM data from the i th received N -continuous GFDM signal. Here, we adopt the way by directly multiplying the decoding matrix \mathbf{P}_w by the i th received N -continuous GFDM signal in (28), which can be expressed by

$$\begin{aligned} \mathbf{P}_w \mathbf{A}^{-1} \tilde{\mathbf{y}}_i &= \mathbf{P}_w \mathbf{A}^{-1} (\bar{\mathbf{x}}_i + \mathbf{H}_i^{-1} \mathbf{n}_i) \\ &= \mathbf{P}_w \mathbf{d}_i + \mathbf{P}_w \mathbf{A}^{-1} \mathbf{w}_i + \mathbf{P}_w \mathbf{A}^{-1} \mathbf{H}_i^{-1} \mathbf{n}_i \\ &= \mathbf{P}_w \mathbf{d}_i + \mathbf{P}_w \mathbf{A}^{-1} \mathbf{Q} \mathbf{P}_f^{-1} (\mathbf{P}_1 \bar{\mathbf{d}}_{i-1} - \mathbf{P}_2 \mathbf{d}_i) + \mathbf{P}_w \mathbf{A}^{-1} \mathbf{H}_i^{-1} \mathbf{n}_i. \end{aligned} \quad (32)$$

Without consideration of the effect the channel noise \mathbf{n}_i , to obtain the $(i-1)$ th data from (32), the following relationship should be satisfied as

$$\mathbf{P}_w = \mathbf{P}_w \mathbf{A}^{-1} \mathbf{Q} \mathbf{P}_f^{-1} \mathbf{P}_2. \quad (33)$$

Then, Eq. (32) is simplified as

$$\mathbf{P}_w \mathbf{A}^{-1} \tilde{\mathbf{y}}_i = \mathbf{P}_w \mathbf{A}^{-1} \mathbf{Q} \mathbf{P}_f^{-1} \mathbf{P}_1 \bar{\mathbf{d}}_{i-1} + \mathbf{P}_w \mathbf{A}^{-1} \mathbf{H}_i^{-1} \mathbf{n}_i. \quad (34)$$

With the exacted $(i - 1)$ th data in (34), similar to (16), (19), and (26), the smooth signal at the receiver can be reconstructed as

$$\begin{aligned} \mathbf{A}^{-1}\mathbf{w}_{i,(r)} &= \mathbf{A}^{-1}\mathbf{P}_w\mathbf{A}^{-1}\tilde{\mathbf{y}}_i - \mathbf{A}^{-1}\mathbf{Q}\mathbf{P}_f^{-1}\mathbf{P}_2\hat{\mathbf{d}}_{i,(r)} \\ &= \mathbf{A}^{-1}\mathbf{P}_w\mathbf{A}^{-1}\mathbf{Q}\mathbf{P}_f^{-1}\mathbf{P}_1\bar{\mathbf{d}}_{i-1} - \mathbf{A}^{-1}\mathbf{Q}\mathbf{P}_f^{-1}\mathbf{P}_2\hat{\mathbf{d}}_{i,(r)} + \mathbf{A}^{-1}\mathbf{P}_w\mathbf{A}^{-1}\mathbf{H}_i^{-1}\mathbf{n}_i. \end{aligned} \quad (35)$$

To obtain the smooth signal from the first two terms in (35), compared to (19) and (26), the following relationship should be satisfied as

$$\mathbf{P}_w\mathbf{A}^{-1}\mathbf{Q}\mathbf{P}_f^{-1} = \mathbf{Q}\mathbf{P}_f^{-1}. \quad (36)$$

According to (33) and (36), we have

$$\mathbf{P}_w = \left(\mathbf{P}_w\mathbf{A}^{-1}\mathbf{Q}\mathbf{P}_f^{-1}\right)\mathbf{P}_2 = \mathbf{Q}\mathbf{P}_f^{-1}\mathbf{P}_2. \quad (37)$$

2) Sufficient Proof

According to (15) and (22)-(25), we have

$$\begin{aligned} \mathbf{P}_2\mathbf{A}^{-1}\mathbf{Q} &= \mathbf{B}\Phi\mathbf{F}\mathbf{A}\mathbf{A}^{-1}\mathbf{Q} \\ &= \mathbf{B}\Phi(\mathbf{F}\mathbf{Q}) \\ &= \begin{bmatrix} \frac{1}{N} \sum_{l=0}^{N-1} F_0(l) & \frac{1}{N} \sum_{l=0}^{N-1} \frac{j2\pi l}{N} F_0(l) & \cdots & \frac{1}{N} \sum_{l=0}^{N-1} \left(\frac{j2\pi l}{N}\right)^V F_0(l) \\ \frac{1}{N} \sum_{l=0}^{N-1} \frac{j2\pi l}{N} F_0(l) & \frac{1}{N} \sum_{l=0}^{N-1} \left(\frac{j2\pi l}{N}\right)^2 F_0(l) & \cdots & \frac{1}{N} \sum_{l=0}^{N-1} \left(\frac{j2\pi l}{N}\right)^{V+1} F_0(l) \\ \vdots & \vdots & \vdots & \vdots \\ \frac{1}{N} \sum_{l=0}^{N-1} \left(\frac{j2\pi l}{N}\right)^V F_0(l) & \frac{1}{N} \sum_{l=0}^{N-1} \left(\frac{j2\pi l}{N}\right)^{V+1} F_0(l) & \cdots & \frac{1}{N} \sum_{l=0}^{N-1} \left(\frac{j2\pi l}{N}\right)^{2V} F_0(l) \end{bmatrix} \\ &= \begin{bmatrix} f(-N_{\text{cp}}) & f_1(-N_{\text{cp}}) & \cdots & f_V(-N_{\text{cp}}) \\ f_1(-N_{\text{cp}}) & f_2(-N_{\text{cp}}) & \cdots & f_{V+1}(-N_{\text{cp}}) \\ \vdots & \vdots & \vdots & \vdots \\ f_V(-N_{\text{cp}}) & f_{V+1}(-N_{\text{cp}}) & \cdots & f_{2V}(-N_{\text{cp}}) \end{bmatrix} \\ &= \mathbf{P}_f. \end{aligned} \quad (38)$$

According to the known relationships in (38) and (37), it can be proved that the two conditions in (33) and (36) can be satisfied.

Therefore, the matrix \mathbf{P}_w in (31) is adopted as the decoding matrix for the signal recovery at the N -continuous GFDM receiver. ■

Finally, with the initialization of $\hat{\mathbf{d}}_{i,(r-1)} = \mathbf{0}_{N \times 1}$, the received data is achieved by the following hard decision as

$$\hat{d}_{i,k,m,(r)} = \arg \min_{d \in \mathcal{C}} \left\{ \left| \hat{y}_{i,k,m,(r)} - d \right|^2 \right\}, \quad (39)$$

where \mathcal{C} denotes the constellation set. Fig. 3 shows the N -continuous GFDM receiver with the interference cancellation.

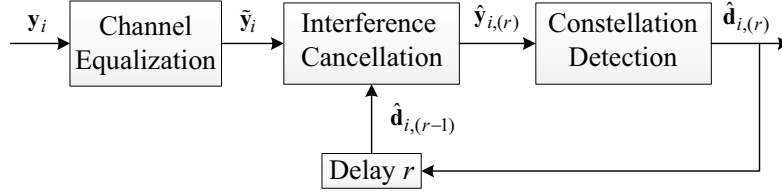


Fig. 3. Block diagram of the N -continuous GFDM receiver.

C. SIR Analysis

In order to observe the effect of the filter-based smooth signal to the GFDM transmission, we analyze the average SIR through evaluating the average power of the smooth signal.

Since the data $d_{i,k,m}$ follows i.i.d. process, we have $E\{\mathbf{d}_i \mathbf{d}_i^H\} = \mathbf{I}_N$ and $E\{\mathbf{d}_i \mathbf{d}_{i-1}^H\} = \mathbf{0}_{N \times N}$, while we let

$$\tilde{\mathbf{P}} = \mathbf{A}^{-1} \mathbf{Q} \mathbf{P}_f^{-1} \mathbf{P}_2 = \mathbf{A}^{-1} \mathbf{P}_w, \quad (40)$$

which is proved to be an idempotent matrix in Appendix A.

Firstly, we investigate the effect of the smooth signal to the average power of the transmitted GFDM signal. Corresponding to the ZF-based GFDM demodulator at the receiver, according to (27) and (40), we have

$$\begin{aligned} E\{\bar{\mathbf{d}}_i \bar{\mathbf{d}}_i^H\} &= E\left\{\mathbf{A}^{-1} \bar{\mathbf{x}}_i (\mathbf{A}^{-1} \bar{\mathbf{x}}_i)^H\right\} \\ &= E\left\{\left(\left(\mathbf{I}_N - \tilde{\mathbf{P}}\right) \mathbf{d}_i + \mathbf{A}^{-1} \mathbf{Q} \mathbf{P}_f^{-1} \mathbf{P}_1 \bar{\mathbf{d}}_{i-1}\right) \left(\left(\mathbf{I}_N - \tilde{\mathbf{P}}\right) \mathbf{d}_i + \mathbf{A}^{-1} \mathbf{Q} \mathbf{P}_f^{-1} \mathbf{P}_1 \bar{\mathbf{d}}_{i-1}\right)^H\right\} \\ &= E\left\{\left(\mathbf{I}_N - \tilde{\mathbf{P}}\right) \mathbf{d}_i \mathbf{d}_i^H \left(\mathbf{I}_N - \tilde{\mathbf{P}}\right)^H\right\} + E\left\{\mathbf{A}^{-1} \mathbf{Q} \mathbf{P}_f^{-1} \mathbf{P}_1 \bar{\mathbf{d}}_{i-1} \bar{\mathbf{d}}_{i-1}^H \left(\mathbf{A}^{-1} \mathbf{Q} \mathbf{P}_f^{-1} \mathbf{P}_1\right)^H\right\} \\ &= \mathbf{I}_N - \tilde{\mathbf{P}} - \tilde{\mathbf{P}}^H + \tilde{\mathbf{P}} \tilde{\mathbf{P}}^H + \hat{\mathbf{P}} E\{\bar{\mathbf{d}}_{i-1} \bar{\mathbf{d}}_{i-1}^H\} \hat{\mathbf{P}}^H, \end{aligned} \quad (41)$$

where

$$\hat{\mathbf{P}} = \mathbf{A}^{-1} \mathbf{Q} \mathbf{P}_f^{-1} \mathbf{P}_1. \quad (42)$$

Moreover, with the initialization of $\bar{\mathbf{d}}_0 = \mathbf{d}_0$, it is easy to obtain that $E\{\bar{\mathbf{d}}_0 \bar{\mathbf{d}}_0^H\} = \mathbf{I}_N$. Thus, Eq. (41) can be further expressed by

$$E\{\bar{\mathbf{d}}_i \bar{\mathbf{d}}_i^H\} = \sum_{i_1=0}^i \hat{\mathbf{P}}^{i_1} \left(\hat{\mathbf{P}}^H\right)^{i_1} - \sum_{i_1=0}^{i-1} \hat{\mathbf{P}}^{i_1} \left(\tilde{\mathbf{P}} + \tilde{\mathbf{P}}^H - \tilde{\mathbf{P}} \tilde{\mathbf{P}}^H\right) \left(\hat{\mathbf{P}}^H\right)^{i_1}. \quad (43)$$

When the roll-off factor of $g(n)$ equals to zero, i.e., $\beta = 0$, it is proved in Appendix B that the elements $\bar{d}_{i,k,m}$ in $\bar{\mathbf{d}}_i$ are also uncorrelated by k and m . Fig. 4 shows that with different roll-off factors and HDOs, the average power of the N -continuous GFDM signal $E\{\bar{\mathbf{d}}_i^H \bar{\mathbf{d}}_i\} = \text{Tr}\{E\{\bar{\mathbf{d}}_i \bar{\mathbf{d}}_i^H\}\}$ varies tiny as i . In other words, for different roll-off factors and HDOs, the average power of the N -continuous GFDM signal can be approximated to be a constant. It is inferred that the smooth signal has a slight effect on the power of the transmitted N -continuous GFDM signal.

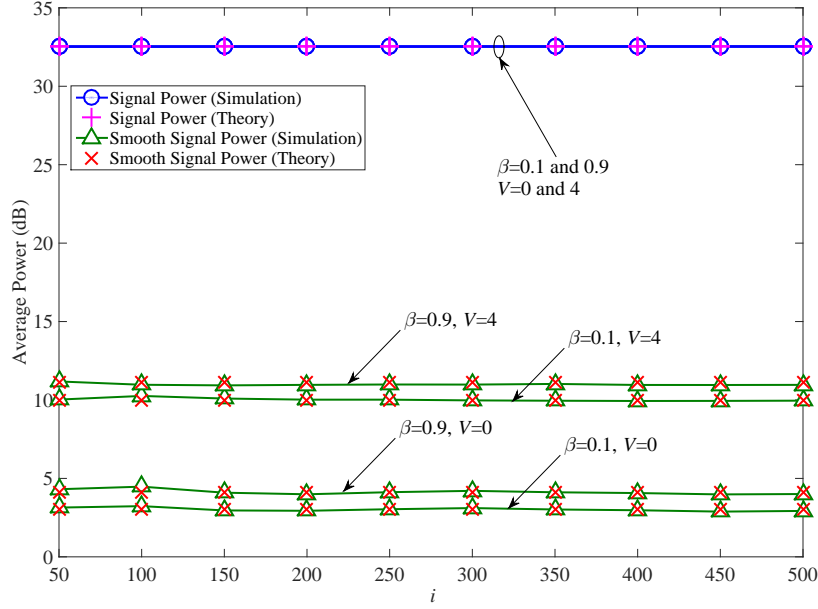


Fig. 4. Average powers of the N -continuous GFDM signal $E\{\bar{\mathbf{d}}_i \bar{\mathbf{d}}_i^H\}$ and the smooth signal $E\{(\mathbf{A}^{-1} \mathbf{w}_i)^H \mathbf{A}^{-1} \mathbf{w}_i\}$ with different roll-off factors β and HDOs V , where the simulation parameters are given in Section IV.

Secondly, under the constant power of the N -continuous GFDM signal, the SIR is analyzed by calculating the average power of the smooth signal $\mathbf{A}^{-1} \mathbf{w}_i$ obtained by the ZF-based GFDM demodulator, expressed by

$$\begin{aligned}
 E\{(\mathbf{A}^{-1} \mathbf{w}_i)^H \mathbf{A}^{-1} \mathbf{w}_i\} &= \text{Tr}\{E\{\mathbf{A}^{-1} \mathbf{w}_i (\mathbf{A}^{-1} \mathbf{w}_i)^H\}\} \\
 &= \text{Tr}\left\{E\left\{\mathbf{A}^{-1} \mathbf{Q} \mathbf{P}_f^{-1} (\mathbf{P}_1 \bar{\mathbf{d}}_{i-1} - \mathbf{P}_2 \mathbf{d}_i) (\mathbf{P}_1 \bar{\mathbf{d}}_{i-1} - \mathbf{P}_2 \mathbf{d}_i)^H (\mathbf{A}^{-1} \mathbf{Q} \mathbf{P}_f^{-1})^H\right\}\right\} \\
 &= \text{Tr}\left\{\hat{\mathbf{P}} E\{\bar{\mathbf{d}}_{i-1} \bar{\mathbf{d}}_{i-1}^H\} \hat{\mathbf{P}}^H + \tilde{\mathbf{P}} \tilde{\mathbf{P}}^H\right\}. \tag{44}
 \end{aligned}$$

Similar to (43), with the initialization of $\mathbf{w}_0 = \mathbf{0}_{N \times 1}$, Eq. (44) can be further expanded to be

$$\begin{aligned}
 E\{(\mathbf{A}^{-1} \mathbf{w}_i)^H \mathbf{A}^{-1} \mathbf{w}_i\} &= \text{Tr}\left\{\hat{\mathbf{P}} E\{\bar{\mathbf{d}}_{i-1} \bar{\mathbf{d}}_{i-1}^H\} \hat{\mathbf{P}}^H + \tilde{\mathbf{P}} \tilde{\mathbf{P}}^H\right\} \\
 &= \text{Tr}\left\{\sum_{i_1=1}^i \hat{\mathbf{P}}^{i_1} (\hat{\mathbf{P}}^H)^{i_1} - \sum_{i_1=1}^{i-1} \hat{\mathbf{P}}^{i_1} (\tilde{\mathbf{P}} + \tilde{\mathbf{P}}^H) (\hat{\mathbf{P}}^H)^{i_1} + \sum_{i_1=0}^{i-1} \hat{\mathbf{P}}^{i_1} \tilde{\mathbf{P}} \tilde{\mathbf{P}}^H (\hat{\mathbf{P}}^H)^{i_1}\right\}. \tag{45}
 \end{aligned}$$

As depicted in Fig. 4, when the observed number of GFDM symbols is increased, i.e., the observation time related to i is longer, the simulated average power of the smooth signal approaches to a constant matching well with the analyzed counterpart in (45). It is implied that the average power of the smooth signal is independent of the time slot index i , and affected by the HDO and the GFDM prototype filter. For an increased roll-off factor or HDO, the average smooth signal power also increases, where HDO is the dominant factor.

Moreover, when $\beta = 0$, according to the relationship between $\hat{\mathbf{P}}$ and $\tilde{\mathbf{P}}$ detailed in Appendix B and the property of idempotent matrix in [25], we have

$$E \left\{ (\mathbf{A}^{-1} \mathbf{w}_i)^H \mathbf{A}^{-1} \mathbf{w}_i \right\} = \text{Tr} \left\{ \hat{\mathbf{P}} \hat{\mathbf{P}}^H + \tilde{\mathbf{P}} \tilde{\mathbf{P}}^H \right\} = 2 \text{Tr} \left\{ \tilde{\mathbf{P}} \right\} = 2 \text{rank} \left\{ \tilde{\mathbf{P}} \right\} = 2(V+1). \quad (46)$$

As shown in Fig. 4, for a small roll-off factor, the average power of the smooth signal approaches to $10 \log_{10}(2V+2)$.

Finally, the SIR between the original GFDM data \mathbf{d}_i and the smooth signal $\mathbf{A}^{-1} \mathbf{w}_i$ is calculated by

$$\gamma_{\text{SIR}} = \frac{\text{Tr} \left\{ E \left\{ \mathbf{d}_i \mathbf{d}_i^H \right\} \right\}}{E \left\{ (\mathbf{A}^{-1} \mathbf{w}_i)^H \mathbf{A}^{-1} \mathbf{w}_i \right\}} = \frac{KM}{\text{Tr} \left\{ \sum_{i_1=0}^{i-1} \hat{\mathbf{P}}^{i_1+1} (\hat{\mathbf{P}}^H)^{i_1+1} - \sum_{i_1=0}^{i-2} \hat{\mathbf{P}}^{i_1+1} \tilde{\mathbf{P}} (\hat{\mathbf{P}}^H)^{i_1+1} + \tilde{\mathbf{P}} \tilde{\mathbf{P}}^H \right\}}. \quad (47)$$

When $\beta = 0$, from (46), γ_{SIR} is derived as

$$\gamma_{\text{SIR}} = \frac{KM}{2(V+1)}. \quad (48)$$

It is concluded that under the constraint of the same number of subcarriers between GFDM and OFDM, the SIR in (48) has M times larger than that in TD-NC-OFDM $K/(2V+2)$ [24]. With the same constraint between GFDM and OFDM above, we can infer that when the roll-off factor of the prototype filter is small, the N -continuous GFDM can still achieve a notable SIR gain compared to the TD-NC-OFDM.

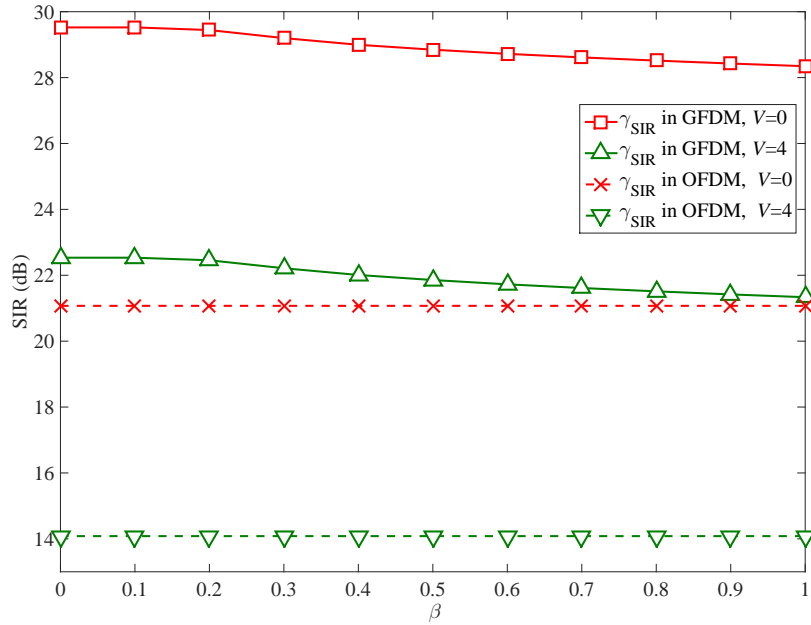


Fig. 5. SIRs of the N -continuous GFDM signal and the TD-NC-OFDM signal with different roll-off factors and HDOs, where the simulation parameters are given in Section IV.

Fig. 5 shows the SIRs versus the roll-off factor β for the varying-HDO N -continuous GFDM and TD-NC-OFDM, where GFDM has the same number of subcarriers as OFDM. For a reduced HDO or roll-off factor, the SIR of N -continuous GFDM is increased, where HDO has the dominant effect on SIR. Moreover, with the small roll-off

factor, compared to TD-NC-OFDM, the enhanced SIR gain of N -continuous GFDM is almost up to M times, where the maximum gain is achieved at $\beta = 0$. It is also implied that for a big M , N -continuous GFDM with a small roll-off filter can achieve much better transmission performance than TD-NC-OFDM, which will be shown in Section IV.

IV. SIMULATION RESULTS

To further characterize our proposed N -continuous-aided GFDM system, we investigated its PSD and BER based on extensive Monte Carlo simulations. The PSD is evaluated by Welch's averaged periodogram method with a 7168-sample Hanning window and 1792-sample overlap after observing 10^5 symbols. The system simulation parameters are summarized in Table I, where the 9-path EVA channel model in 3GPP LTE is adopted [26], whose channel delay and channel power are [0, 30, 150, 310, 370, 710, 1090, 1730, 2510] ns and [0, -1.5, -1.4, -3.6, -0.6, -9.1, -7.0, -12.0, -16.9] dB, respectively. To avoid the lengths of the window edges in the windowing technique for GFDM [17] exceeding the given lengths of CP and cyclic postfix, the roll-off factor of the window in the windowing technique is set to be $\alpha = 0.015$, where the lengths of both CP and cyclic postfix are 140.

TABLE I
SIMULATION PARAMETERS

Parameters	Values
Constellation modulation	16QAM
Transmitter filter	RC
Roll-off factor (β)	0.1
Number of subcarriers (K)	256
Number of subsymbols (M)	7
Time-domain oversampling factor	4
Frequency interval (Δf)	15 KHz
Sampling interval	9.3 ns
Carrier frequency	2 GHz
Maximum Doppler shift (f_D)	100 Hz
Length of CP in GFDM	280
Length of CP in OFDM	280
Channel environment	Multipath Rayleigh fading channel

Fig. 6 compares the PSDs among conventional OFDM, conventional GFDM, the windowing technique in GFDM, the TD-NC-OFDM, and the N -continuous GFDM with different HDOs. It is shown that with the HDO increasing, the sidelobe suppression performance of the N -continuous GFDM is significantly improved. Furthermore, the N -continuous GFDM achieves more rapid sidelobe decaying than the TD-NC-OFDM, since the transmit filter in GFDM has much lower sidelobes than that in the rectangularly pulsed OFDM. With a small HDO, the windowing technique has a more compact spectrum than the N -continuous GFDM. On the contrary, for a big HDO, the N -continuous GFDM has the lowest out-of-band radiation. For example, when $V = 6$, the N -continuous GFDM has more rapid sidelobe decaying than the TD-NC-OFDM and the windowing technique.

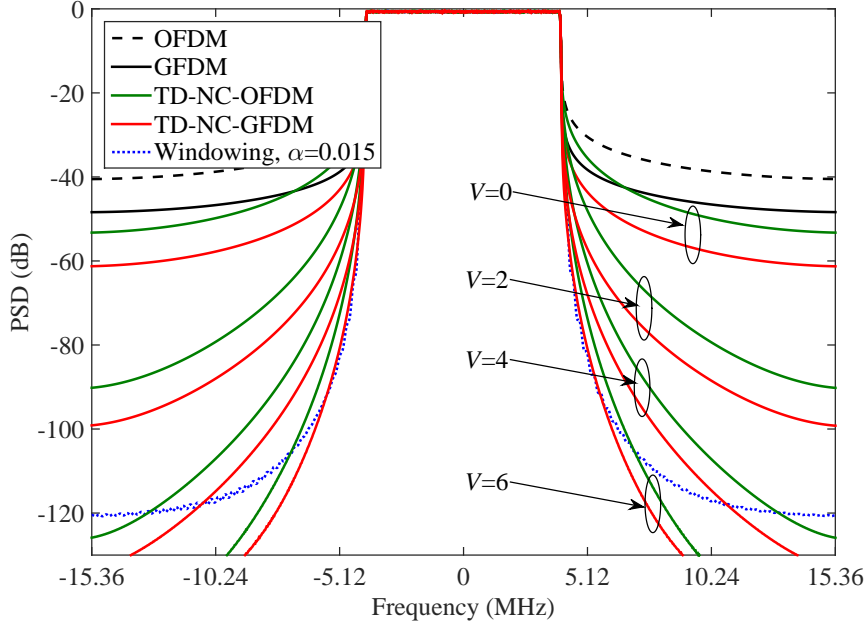


Fig. 6. PSD comparison among OFDM, GFDM, TD-NC-OFDM, the windowing technique, the N -continuous GFDM.

In Figs. 7 and 8, we plot the BER curves of OFDM, GFDM, the TD-NC-OFDM, and the N -continuous GFDM in AWGN channel and multipath Rayleigh fading channel, respectively. The number of iterations of the proposed signal recovery algorithm in the N -continuous GFDM is set to be 8 with the HDO parameters $V = 0, 2, 4$. Observe in Figs. 7 and 8 that upon increasing the HDO, the error floor caused by the increased smooth signal, which is effectively eliminated by the signal recovery algorithm and has the BER close to conventional GFDM. More importantly, without consideration of the signal recovery for interference cancellation, the N -continuous GFDM achieves much better BER performance than the TD-NC-OFDM, which matches well with the SIR analysis in Section III-C, while maintaining excellent sidelobe suppression performance as shown in Fig. 6.

Furthermore, since the parameter HDO is the dominate thing in SIR as analyzed in Section III-C, considering a big HDO of $V = 6$, in Fig. 9, we investigate the BER performance of the N -continuous GFDM compared to the TD-NC-OFDM and the windowing technique, where the TD-NC-OFDM adopts the signal recovery algorithm with 8 iterations in [24]. It is denoted in Fig. 9 that a high BER performance floor is induced by the smooth signal in both the N -continuous GFDM and the TD-NC-OFDM, where the former still has a large error performance gain than the latter. Under the constraint of a fixed number of iterations for signal recovery, the data conveyed by the TD-NC-OFDM cannot be well detected, while the BER of the N -continuous GFDM can be significantly reduced, which is also lower than that of the windowing technique.

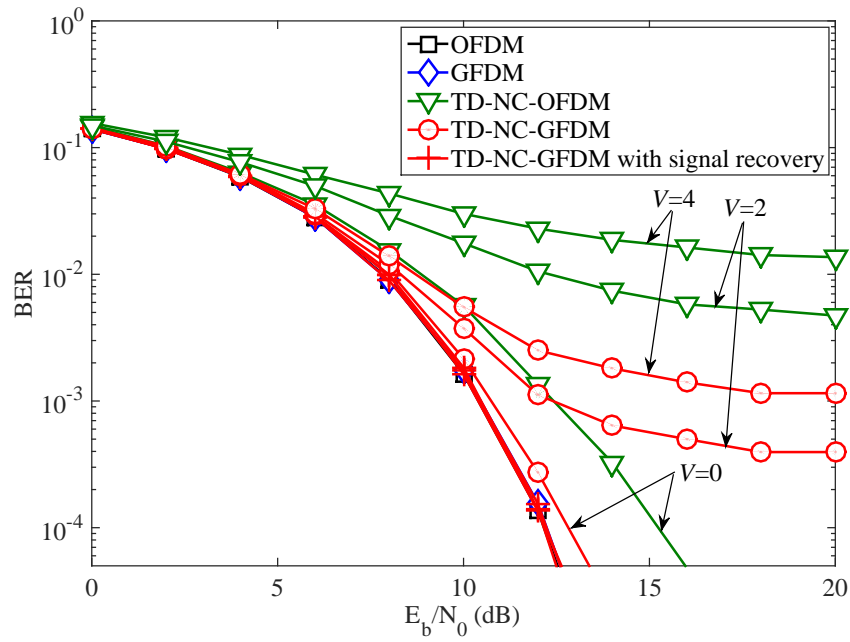


Fig. 7. BERs of conventional OFDM, conventional GFDM, TD-NC-OFDM, and N -continuous GFDM in AWGN channel.

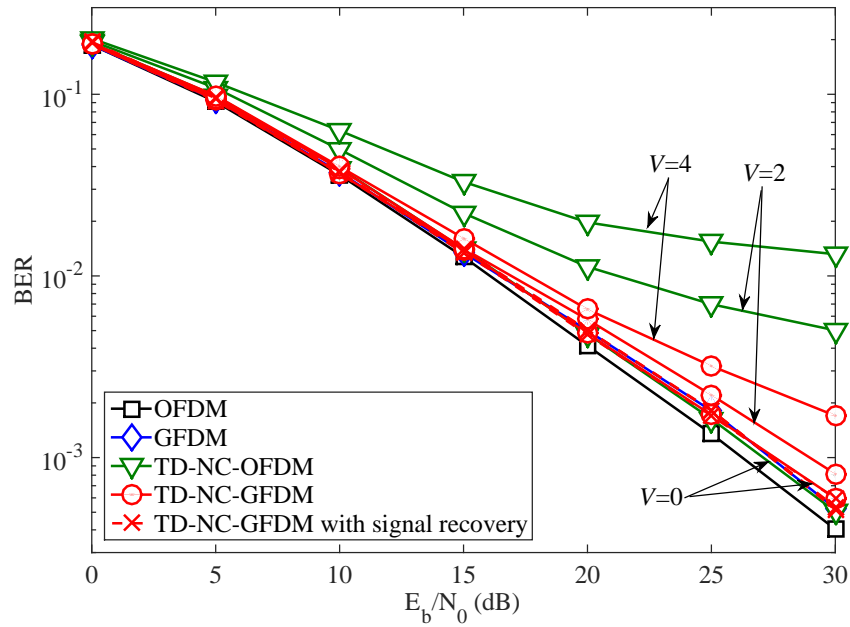


Fig. 8. BERs of conventional OFDM, conventional GFDM, TD-NC-OFDM, and N -continuous GFDM in Rayleigh fading channel.

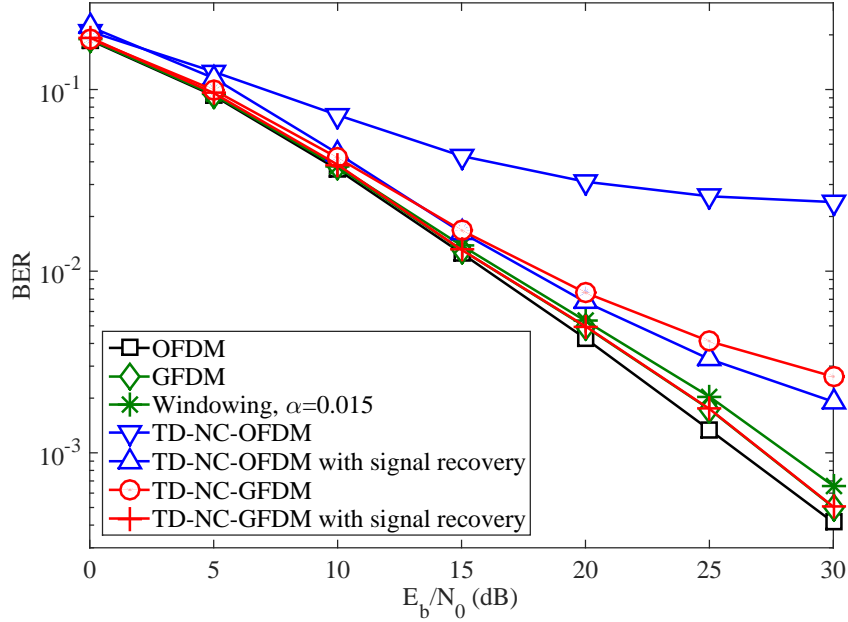


Fig. 9. BERs of TD-NC-OFDM, N -continuous GFDM, and the windowing technique for GFDM in Rayleigh fading channel, where $V = 6$.

V. CONCLUSION

In this paper, we have proposed an N -continuous aided GFDM system model for sidelobe suppression, relying on the smooth principle of TD-NC-OFDM. Based on the design of the generalized basis signals, the proposed N -continuous GFDM signaling is capable of dramatically suppress the spectral leakage over a block of subcarriers. Furthermore, we carried out its SIR analysis to evaluate the effect of the smooth signal on the received signal, where the N -continuous GFDM can obtain a higher SIR than the TD-NC-OFDM when the number of GFDM subsymbol is larger than 1 and the same number of subcarriers in GFDM and OFDM is considered. Finally, by constructing a decoding matrix according to the N -continuous GFDM signaling architecture, we investigated a signal recovery algorithm at the receiver, which is free from an error floor. Our simulation results demonstrated that the proposed N -continuous GFDM scheme has the explicit benefits of better sidelobe suppression and lower BER than those of the TD-NC-OFDM.

APPENDIX A

PROPERTIES OF MATRIX $\tilde{\mathbf{P}}$ IN (40)

From (38), we can derive that

$$\tilde{\mathbf{P}}^2 = \mathbf{A}^{-1} \mathbf{Q} \mathbf{P}_f^{-1} \mathbf{P}_2 \mathbf{A}^{-1} \mathbf{Q} \mathbf{P}_f^{-1} \mathbf{P}_2 = \mathbf{A}^{-1} \mathbf{Q} \mathbf{P}_f^{-1} \mathbf{P}_f \mathbf{P}_f^{-1} \mathbf{P}_2 = \tilde{\mathbf{P}}, \quad (49)$$

which denotes that $\tilde{\mathbf{P}}$ is idempotent.

APPENDIX B

PROOF OF THE INDEPENDENCE AMONG ELEMENTS IN $\bar{\mathbf{d}}_{i,k,m}$ FOR $\beta = 0$

When $\beta = 0$, the prototype filter $g(n)$ becomes a Dirichlet function. Thus, under the constraint of the normalized energy of $g(n)$, i.e., $\sum_{n=0}^{N-1} |g(n)|^2 = 1$, the transmitter matrix \mathbf{A} can be expressed by

$$\mathbf{A} = \frac{1}{N} \mathbf{F}^H \begin{bmatrix} \Phi_0 \mathbf{C} & \Phi_1 \mathbf{C} & \cdots & \Phi_{M-1} \mathbf{C} \end{bmatrix}, \quad (50)$$

where $\Phi_m = \text{diag} \left(e^{-j2\pi \frac{m}{M} 0} \ e^{-j2\pi \frac{m}{M} 1} \ \cdots \ e^{-j2\pi \frac{m}{M} (N-1)} \right)$,

$$\mathbf{C} = \begin{bmatrix} \mathbf{c} & & & \\ & \mathbf{c} & & \\ & & \ddots & \\ & & & \mathbf{c} \end{bmatrix}_{N \times K}, \quad (51)$$

and $\mathbf{c} = \sqrt{K} [1 \ 1 \ \cdots \ 1]^T$ is an $M \times 1$ vector.

According to (50) and (51), we can derive that

$$\mathbf{A}^H \mathbf{A} = \frac{1}{N} \begin{bmatrix} \mathbf{C}^H \Phi_0^H \Phi_0 \mathbf{C} & \mathbf{C}^H \Phi_0^H \Phi_1 \mathbf{C} & \cdots & \mathbf{C}^H \Phi_0^H \Phi_{M-1} \mathbf{C} \\ \mathbf{C}^H \Phi_1^H \Phi_0 \mathbf{C} & \mathbf{C}^H \Phi_1^H \Phi_1 \mathbf{C} & \cdots & \mathbf{C}^H \Phi_1^H \Phi_{M-1} \mathbf{C} \\ \vdots & \vdots & \ddots & \vdots \\ \mathbf{C}^H \Phi_{M-1}^H \Phi_0 \mathbf{C} & \mathbf{C}^H \Phi_{M-1}^H \Phi_1 \mathbf{C} & \cdots & \mathbf{C}^H \Phi_{M-1}^H \Phi_{M-1} \mathbf{C} \end{bmatrix}. \quad (52)$$

In (52), according to the structure of \mathbf{C} in (51), $\mathbf{C}^H \Phi_m^H \Phi_{m'} \mathbf{C}$ is a diagonal matrix with its $(k+1)$ th row and $(k+1)$ th column element given by

$$K \sum_{l=kM}^{(k+1)M-1} e^{j2\pi \frac{m-m'}{M} l} = K \frac{1 - e^{j2\pi(m-m')}}{1 - e^{j2\pi \frac{m-m'}{M}}} = \begin{cases} KM, & m = m', \\ 0, & m \neq m', \end{cases} \quad (53)$$

where $k = 0, 1, \dots, K-1$ and $m, m' = 0, 1, \dots, M-1$. Thus, Eq. (52) can be simplified as

$$\mathbf{A}^H \mathbf{A} = \mathbf{I}_N, \quad (54)$$

which denotes that when $\beta = 0$, $\mathbf{A}^H = \mathbf{A}^{-1}$.

Based on the mathematical induction, with the initialization of $E \{ \bar{\mathbf{d}}_0 \bar{\mathbf{d}}_0^H \} = \mathbf{I}_N$, we assume that $E \{ \bar{\mathbf{d}}_{i-1} \bar{\mathbf{d}}_{i-1}^H \} = \mathbf{I}_N$. According to (41), we have

$$E \{ \bar{\mathbf{d}}_i \bar{\mathbf{d}}_i^H \} = \mathbf{I}_N - \tilde{\mathbf{P}} - \tilde{\mathbf{P}}^H + \tilde{\mathbf{P}} \tilde{\mathbf{P}}^H + \hat{\mathbf{P}} \hat{\mathbf{P}}^H. \quad (55)$$

Based on \mathbf{P}_1 in (21) and \mathbf{P}_2 in (22), it can be proved that $\mathbf{P}_1 \mathbf{P}_1^H = \mathbf{P}_2 \mathbf{P}_2^H$. Thus, Eq. (55) can be further written by

$$E \{ \bar{\mathbf{d}}_i \bar{\mathbf{d}}_i^H \} = \mathbf{I}_N - \tilde{\mathbf{P}} - \tilde{\mathbf{P}}^H + 2\tilde{\mathbf{P}} \tilde{\mathbf{P}}^H. \quad (56)$$

Additionally, from (40) and (38), we have

$$\mathbf{P}_2 \tilde{\mathbf{P}} = \mathbf{P}_2. \quad (57)$$

According to the relationship above, multiplying $E \{\bar{\mathbf{d}}_i \bar{\mathbf{d}}_i^H\}$ in (56) left by \mathbf{P}_2 and right by \mathbf{P}_2^H gives

$$\mathbf{P}_2 E \{\bar{\mathbf{d}}_i \bar{\mathbf{d}}_i^H\} \mathbf{P}_2^H = \mathbf{P}_2 \mathbf{P}_2^H. \quad (58)$$

by employing a singular value decomposition (SVD) of \mathbf{P}_2 as $\mathbf{P}_2 = \mathbf{U} \mathbf{\Lambda} \mathbf{V}^H$, Eq. (58) is rewritten by

$$\mathbf{V}_{V+1}^H E \{\bar{\mathbf{d}}_i \bar{\mathbf{d}}_i^H\} \mathbf{V}_{V+1} = \mathbf{I}_{V+1}, \quad (59)$$

where \mathbf{U} is a $(V+1) \times (V+1)$ unitary matrix, $\mathbf{\Lambda} = [\text{diag}(\lambda_0 \lambda_1 \cdots \lambda_V) \mathbf{0}_{(V+1) \times (N-V-1)}]$, \mathbf{V} is an $N \times N$ unitary matrix, and \mathbf{V}_{V+1} is composed of the first $V+1$ columns of \mathbf{V} .

Based on the property of the unitary matrix, that is its columns form an orthonormal basis, considering $E \{\bar{\mathbf{d}}_i \bar{\mathbf{d}}_i^H\}$ as the linear mapping matrix between \mathbf{V}_{V+1}^H and \mathbf{V}_{V+1} , we can obtain

$$E \{\bar{\mathbf{d}}_i \bar{\mathbf{d}}_i^H\} = \mathbf{I}_N, \quad (60)$$

which implies that when $\beta = 0$, the data $\bar{d}_{i,k,m}$ are uncorrelated.

REFERENCES

- [1] G. Fettweis, M. Krondorf, and S. Bittner, "GFDM—Generalized frequency division multiplexing," in *Proc. 69th IEEE VTC Spring*, Barcelona, Spain, Apr. 2009, pp. 1-4.
- [2] R. Datta, N. Michailow, M. Lentmaier, and G. Fettweis, "GFDM interference cancellation for flexible cognitive radio PHY design," in *Proc. 76th IEEE VTC Fall*, Québec City, QC, Canada, Sep. 2012, pp. 1-5.
- [3] I. Gaspar, N. Michailow, A. Navarro, E. Ohlmer, S. Krone, and G. Fettweis, "Low complexity GFDM receiver based on sparse frequency domain processing," in *Proc. 77th IEEE VTC Spring*, Dresden, Germany, Jun. 2013, pp. 1-6.
- [4] G. Wunder, P. Jung, M. Kasparick, T. Wild, F. Schaich, Y. Chen, S. Brink, I. Gaspar, N. Michailow, A. Festag, L. Mendes, N. Cassiau, D. Ktenas, M. Dryjanski, S. Pietrzyk, B. Eged, P. Vago, and F. Wiedmann, "5GNOW: Non-orthogonal, asynchronous waveforms for future mobile applications," *IEEE Commun. Mag.*, vol. 52, no. 2, pp. 97-105, Feb. 2014.
- [5] M. Matthe, L. L. Mendes, and G. Fettweis, "Generalized frequency division multiplexing in a Gabor transform setting," *IEEE Commun. Letters*, vol. 18, no. 8, pp. 1379-1382, Aug. 2014.
- [6] H. Lin and P. Siohan, "Orthogonality improved GFDM with low complexity implementation," *2015 IEEE Wireless Commun. Networking Conf. (WCNC)*, New Orleans, United states, Jun. 2015, pp. 597-602.
- [7] B. Farhang-Boroujeny and H. Moradi, "Derivation of GFDM based on OFDM principles," *2015 IEEE Int. Conf. Commun. (ICC)*, London, England, Jun. 2015, pp. 2680-2685.
- [8] A. Farhang, N. Marchetti, and L. E. Doyle, "Low complexity GFDM receiver design: a new approach," *2015 IEEE Int. Conf. Commun. (ICC)*, London, England, Jun. 2015, pp. 4775-4780.
- [9] A. Farhang, N. Marchetti, and L. E. Doyle, "Low complexity modem design for GFDM," *IEEE Trans. Signal Process.*, vol. 64, no. 6, pp. 1507-1518, Mar. 2016.
- [10] A. Nimr, D. Zhang, A.-B. Martinez, and G. Fettweis, "A study on the physical layer performance of GFDM for high throughput wireless communication," in *Proc. 25th European Signal Processing Conference (EUSIPCO)*, Kos, Greece, Aug. 2017, pp. 668-672.
- [11] P.-C. Chen, B. Su, and Y. Huang, "Matrix characterization for GFDM: low complexity MMSE receivers and optimal filters," *IEEE Trans. Signal Process.*, vol. 65, no. 18, pp. 4940-4955, Sep. 2017.
- [12] E. Öztürk, E. Basar, and H. A. Çirpan, "Generalized frequency division multiplexing with flexible index modulation," *IEEE Access*, vol. 5, pp. 24727-24746, Oct. 2017.
- [13] Y. Medjahdi, S. Traverso, R. Gerzaguet, H. Shaïek, R. Zayani, D. Demmer, R. Zakaria, J.-B. Doré, M. B. Mabrouk, D. L. Ruyet, Y. Louët, and D. Roviras, "On the road to 5G: comparative study of physical layer in MTC context," *IEEE Access*, vol. 5, pp. 26556-26581, Nov. 2017.
- [14] S. Tiwari and S. S. Das, "Low-complexity joint-MMSE GFDM receiver," *IEEE Trans. Commun.*, vol. 66, no. 4, pp. 1661-1674, 2018.

- [15] M. Kasparick, G. Wunder, C. F. Schaich, T. Wild, V. Berg, N. Cassiau, J. Dor, D. Ktnas, M. Dryjaski, S. Pietrzyk, I. S. Gaspar, and N. Michailow, "5G waveform candidate selection," Tech. Rep., D3.1 of 5G-Now, FP7 European Research Project, Nov. 2013.
- [16] R. Datta, G. Fettweis, Y. Futatsugi, and M. Ariyoshi, "Comparative analysis on interference suppressive transmission schemes for white space radio access," in *Proc. 75th IEEE VTC Spring*, Yokohama, Japan, May 2012.
- [17] N. Michailow, M. Matth e, I. Gaspar, A. Navarro Caldevilla, L. L. Mendes, A. Festag, and G. Fettweis, "Generalized frequency division multiplexing for 5th generation cellular networks," *IEEE Trans. on Commun.*, vol. 62, no. 9, pp. 3045-3061, Sep. 2014.
- [18] B. Farhang-Boroujeny, A. Farhang, A. R. Reyhani, A. Aminjavaheri, and D. Qu, "A comparison of linear FBMC and circularly shaped waveforms," in *Proc. 2016 IEEE/ACES International Conference on Wireless Information Technology and Systems (ICWITS) and Applied Computational Electromagnetics (ACES)*, Honolulu, HI, USA, Mar. 2016, pp. 1-2.
- [19] M. Matth e, N. Michailow, I. Gaspar, and G. Fettweis, "Influence of pulse shaping on bit error rate performance and out of band radiation of generalized frequency division multiplexing," presented at the Internal Conf. Communications Workshop 5G Technologies, Sydney, NSW, Australia, Jun. 2014.
- [20] J. van de Beek and F. Berggren, " N -continuous OFDM," *IEEE Commun. Lett.*, vol. 13, no. 1, pp. 1-3, Jan. 2009.
- [21] J. van de Beek, "Sculpting the multicarrier spectrum: a novel projection precoder," *IEEE Commun. Lett.*, vol. 13, no. 12, pp. 881-883, Dec. 2009.
- [22] J. van de Beek, "Orthogonal multiplexing in a subspace of frequency well-localized signals," *IEEE Commun. Lett.*, vol. 14, no. 10, pp. 882-884, Oct. 2010.
- [23] P. Wei, L. Dan, Y. Xiao, and S. Li, "A low-complexity time-domain signal processing algorithm for N -continuous OFDM," in *Proc. IEEE Int. Conf. Commun. (ICC)*, Budapest, Hungary, Jun. 2013, pp. 5754-5758.
- [24] P. Wei, L. Dan, Y. Xiao, W. Xiang, and S. Li, "Time-domain N -continuous OFDM: System architecture and performance analysis," *IEEE Trans. Veh. Technol.*, vol. 66, no. 3, pp. 2394-2407, Mar. 2017.
- [25] G. Strang, *Linear Algebra and its Applications*, 3rd ed. San Diego, CA: Harcourt Brace Jovanovich Publishers, 1976.
- [26] *User Equipment (UE) radio transmission and reception (Release 15)*, 3GPP TS 36.101, v15.0.0, Sep. 2017. [Online]. Available: <http://www.3gpp.org/>.